PAPER • OPEN ACCESS

Active buckling control of an imperfect beam-column with circular cross-section using piezo-elastic supports and integral LQR control

To cite this article: Maximilian Schaeffner and Roland Platz 2016 *J. Phys.: Conf. Ser.* **744** 012165

View the article online for updates and enhancements.

Active buckling control of an imperfect beam-column with circular cross-section using piezo-elastic supports and integral LQR control

Maximilian Schaeffner[1] **and Roland Platz**[2]

[1] System Reliability and Machine Acoustics SzM, Technische Universität Darmstadt, Magdalenenstraße 4, D-64289 Darmstadt, Germany
[2] Fraunhofer Institute for Structural Durability and System Reliability LBF, Bartningstraße 47, D-64289 Darmstadt, Germany

E-mail: `schaeffner@szm.tu-darmstadt.de`

Abstract. For slender beam-columns loaded by axial compressive forces, active buckling control provides a possibility to increase the maximum bearable axial load above that of a purely passive structure. In this paper, the potential of active buckling control of an imperfect beam-column with circular cross-section using piezo-elastic supports is investigated numerically. Imperfections are given by an initial deformation of the beam-column caused by a constant imperfection force. With the piezo-elastic supports, active bending moments in arbitrary directions orthogonal to the beam-column's longitudinal axis can be applied at both beam-column's ends. The imperfect beam-column is loaded by a gradually increasing axial compressive force resulting in a lateral deformation of the beam-column. First, a finite element model of the imperfect structure for numerical simulation of the active buckling control is presented. Second, an integral linear-quadratic regulator (LQR) that compensates the deformation via the piezo-elastic supports is derived for a reduced modal model of the ideal beam-column. With the proposed active buckling control it is possible to stabilize the imperfect beam-column in arbitrary lateral direction for axial loads above the theoretical critical buckling load and the maximum bearable load of the passive structure.

1. Introduction

Buckling of slender and compressively loaded beam-columns is a critical failure mode in the design of light-weight structures. The theory of buckling for passive beam-columns has been thoroughly investigated, [1]. Real, non-ideal or imperfect beam-columns exhibit large lateral deformations for axial loads considerably below the theoretical critical buckling load and, therefore, have lower maximum bearable axial loads. A general approach to passively increase the maximum bearable axial load is to change the geometry, e. g. length and cross-section area, or the material so that the beam-column withstands higher loads. This, however, is sometimes not desirable because of given design constraints. In these cases, active buckling control without significant change in the beam-column's geometry and material provides a suitable approach to increase the maximum bearable axial load of a given structure.

Active buckling control of slender beam-columns with rectangular cross-section and different boundary conditions has been investigated numerically and experimentally several times, [2, 3, 4, 5, 6, 7, 8]. The investigated structures had relatively high slenderness ratios s, with

$300 \leq s \leq 1\,760$ and low theoretical critical buckling loads. Often, surface bonded piezoelectric patches were applied to beam-columns with rectangular cross-section to induce active bending moments that counteract the deformation, [2, 3, 4, 5, 6]. The active stabilization concept investigated by earlier own studies [7, 8] used piezoelectric stack actuators to apply active lateral forces near the base of a fixed-pinned beam-column with rectangular cross-section. Compared to other studies mentioned above, most of the beam-column's surface was kept free from any actuator like piezoelectric patches and only strain gauges were applied to the surface. In [7, 8] and additional to all other studies, a lateral disturbance force representing uncertainty in the beam-column's loading was introduced to investigate the approach of active buckling control with lateral forces near the base of the fixed-pinned beam-column. In an experimental study, an increase in the critical axial buckling load of 40 % was achieved by using a linear-quadratic regulator (LQR) to control the first three lateral deflection modes of the supercritically loaded beam-column, [8].

To the authors' knowledge, active buckling control of beam-columns with circular cross-section has not been investigated so far except in own works, [9, 10]. In [9], active buckling control of a circular beam-column with active lateral forces acting near the beam-column's fixed base was investigated numerically and an increase of 110 % in the critical buckling load was achieved. The studies mentioned before investigated beam-columns with high slenderness ratios $300 \leq s \leq 1\,760$ and relatively low buckling loads. In this paper, active buckling control of a relatively stiff beam-column with circular cross-section and relatively low and realistically more often applied slenderness ratio $s = 108$ is investigated numerically. A new concept for piezo-elastic supports is used. Lateral forces of piezoelectric stack actuators are transformed into bending moments acting in arbitrary directions at the beam-column ends. By that, the beam-column surface is kept entirely free of any actuators. In [10], active buckling control by LQR control for this beam-column system without imperfections loaded by a constant axial force was simulated numerically. A lateral impulse disturbance force was used to initially deform the ideal beam-column and an increase of 247 % in the critical buckling load was achieved by LQR control. In an experimental test setup, the real imperfections had a significant influence on the active buckling control and the standard LQR proved to be insufficient. Therefore, an integral LQR will now be used to compensate the deformation of the imperfect beam-column caused by a constant imperfection force. In the following, first the investigated beam-column system with piezo-elastic supports and a mathematical model of the imperfect structure are presented. Second, a reduced modal model of the axially loaded beam-column for design of the integral LQR is derived. Finally numerical simulations of the active buckling control and conclusions are presented.

2. System description and mathematical model
In this section, the beam-column system and a state space finite element (FE) model of the imperfect structure for numerical simulation and controller design are presented.

2.1. Beam-column system with piezo-elastic supports
The investigated system is a slender beam-column made of aluminum alloy EN AW-7075 with length l_b. It has a circular solid cross-section of radius r_b, bending stiffness EI_b and density ϱ_b, all assumed to be constant across the entire beam-column length, figure 1. The beam-column has two piezo-elastic supports A at $x = 0$ and B at $x = l_\mathrm{b}$. The concept of the piezo-elastic supports was first presented in [10] and a model validation was performed in [11]. The central element of the support is an elastic spring element that is represented by rotational stiffness $k_{\varphi_y,\mathrm{A}} = k_{\varphi_z,\mathrm{A}} = k_{\varphi_y,\mathrm{B}} = k_{\varphi_z,\mathrm{B}} = k_\mathrm{r}$ and lateral stiffness $k_{y,\mathrm{A}} = k_{z,\mathrm{A}} = k_{y,\mathrm{B}} = k_{z,\mathrm{B}} = k_\mathrm{l}$ that are the same for both supports A and B and in both y- and z-direction. In each piezo-elastic support A and B at $x = -l_\mathrm{ext}$ and $x = l_\mathrm{b} + l_\mathrm{ext}$, three piezoelectric stack actuators are arranged

in a support housing at an angle of $120°$ to each other in one plane orthogonal to the beam-column's x-axis. They are connected to the beam-column via a relatively stiff axial extension (grey) made of hardened steel 1.2312 with length l_{ext}, radius r_{ext}, bending stiffness EI_{ext} and density ϱ_{ext} creating cantilever beam ends beyond both elastic spring elements. This way, active lateral forces in arbitrary directions orthogonal to the beam-column's longitudinal x-axis are transformed into bending moments acting in arbitrary directions at the beam-column ends in both piezo-elastic supports A and B.
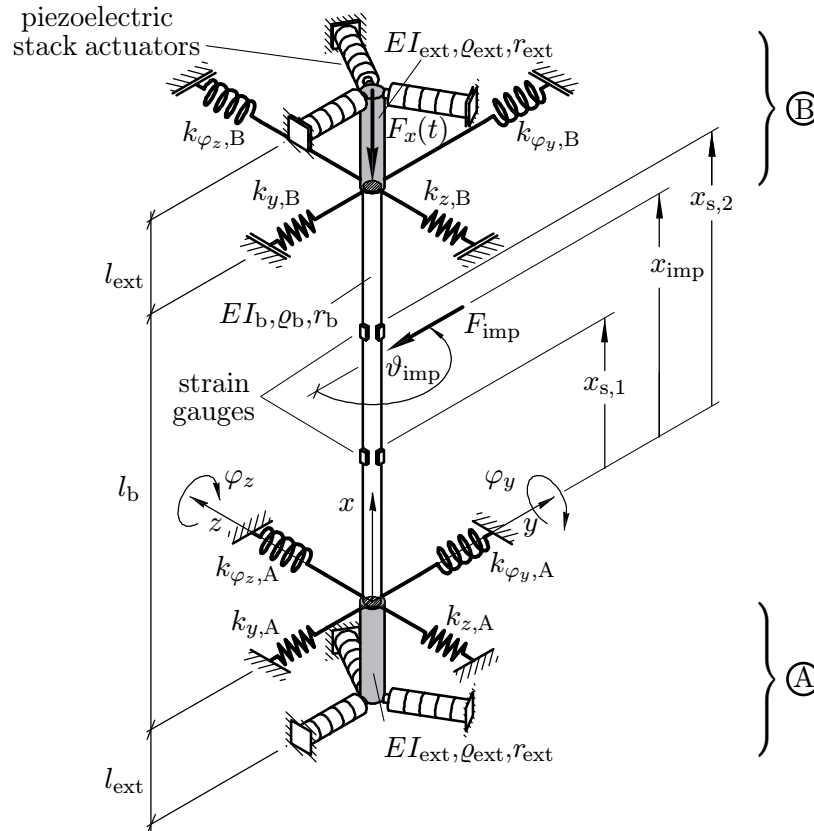

Figure 1: Sketch of beam-column system.

At the upper support B at $x = l_{\text{b}}$, a gradually increasing axial load $F_x(t)$ is applied. To represent imperfections such as predeformation, eccentric loading or clamping moments that are present in real structures, the otherwise ideal beam-column is deformed by a constant lateral imperfection force F_{imp} with variable angle $0° \leq \vartheta_{\text{imp}} \leq 360°$ acting at $x_{\text{imp}} = l_{\text{b}}/2$. This way, the dynamic behavior of an ideal or perfect beam-column with an additional external imperfection force is assumed to be the same as the dynamic behavior of a real, imperfect structure. To determine the deformation of the beam-column in an experimental test setup, it is assumed in the model that strain gauges at positions $x_{\text{s},1/2}$ measure the surface strain of the beam-column in y- and z-direction. The parameters of the beam-column system presented in figure 1 are summarized in table 1. The values for the spring element's rotational stiffness k_{r} and lateral stiffness k_{l} were obtained from static stiffness measurements on a material testing machine, [11].

Table 1: Properties of beam-column system.

property	symbol	value	SI-unit
beam-column length	l_b	$400.0 \cdot 10^{-3}$	m
beam-column radius	r_b	$4.0 \cdot 10^{-3}$	m
beam-column density	ϱ_b	$2\,789.0$	kg/m^3
beam-column Young's modulus	E_b	$75.8 \cdot 10^{9}$	N/m^2
axial extension length	l_ext	$7.5 \cdot 10^{-3}$	m
axial extension radius	r_ext	$6.0 \cdot 10^{-3}$	m
axial extension density	ϱ_ext	$7\,810.0$	kg/m^3
axial extension Young's modulus	E_ext	$210.0 \cdot 10^{9}$	N/m^2
spring element rotational stiffness	k_r	192.4	Nm/rad
spring element lateral stiffness	k_l	$30.0 \cdot 10^{6}$	N/m
piezoelectric stack actuator lateral stiffness	k_p	$22.0 \cdot 10^{6}$	N/m
strain gauge position 1	$x_\mathrm{s,1}$	$148.0 \cdot 10^{-3}$	m
strain gauge position 2	$x_\mathrm{s,2}$	$252.0 \cdot 10^{-3}$	m
modal damping ratio mode 1	ζ_1	$15.0 \cdot 10^{-3}$	–
modal damping ratio mode 2	ζ_2	$4.5 \cdot 10^{-3}$	–

2.2. Finite Element model

The beam-column and the stiff axial extensions are discretized by $N-1$ one-dimensional EULER-BERNOULLI beam elements of length l_el with N nodes. Each node n is described by the lateral displacements v_n and w_n in y- and z-direction and the rotational displacements $\varphi_{y,n}$ and $\varphi_{z,n}$ around the y- and z-axis, figure 2a. Axial and rotational displacements in and around the x-axis of the beam-column are neglected. Figure 2b shows the discretized beam-column with $N-1$ finite elements and N nodes. The axial extensions are discretized by one single finite element, so that the axial load $F_x(t)$ acts at node $n = N - 1$. The piezoelectric stack actuators in the piezo-elastic supports A and B are represented by lateral stiffness k_p and additional active control forces $F_{\mathrm{a}y/z,\mathrm{A/B}}(t)$ in y- and z-direction of nodes $n = 1$ and $n = N$ of the FE model. The constant imperfection force F_imp with angle $0\,° \leq \vartheta_\mathrm{imp} \leq 360\,°$ acts on the central node n_c at $x_\mathrm{imp} = l_\mathrm{b}/2$.

The GALERKIN method with cubic HERMITIAN shape functions $\boldsymbol{g}(x_\mathrm{el})$ is used to get the element mass matrix $\boldsymbol{M}_\mathrm{el}$, elastic element stiffness matrix $\boldsymbol{K}_\mathrm{e,el}$ and geometric element stiffness matrix $\boldsymbol{K}_\mathrm{g,el}$, all $[8 \times 8]$, for the EULER-BERNOULLI beam elements, [12]. The element mass matrix $\boldsymbol{M}_\mathrm{el}$ and elastic element stiffness matrix $\boldsymbol{K}_\mathrm{e,el}$ are readily found in literature, [12, 13]. The geometric element stiffness matrix

$$
\boldsymbol{K}_\mathrm{g,el} = \frac{1}{l_\mathrm{el}}
\begin{pmatrix}
6/5 & 0 & 0 & l_\mathrm{el}/10 & -6/5 & 0 & 0 & l_\mathrm{el}/10 \\
 & 6/5 & -l_\mathrm{el}/10 & 0 & 0 & -6/5 & -l_\mathrm{el}/10 & 0 \\
 & & 2/15\,l_\mathrm{el}^2 & 0 & 0 & l_\mathrm{el}/10 & -l_\mathrm{el}^2/30 & 0 \\
 & & & 2/15\,l_\mathrm{el}^2 & -l_\mathrm{el}/10 & 0 & 0 & -l_\mathrm{el}^2/30 \\
 & & & & 6/5 & 0 & 0 & -l_\mathrm{el}/10 \\
 & & & & & 6/5 & l_\mathrm{el}/10 & 0 \\
 & \text{symmetric} & & & & & 2/15\,l_\mathrm{el}^2 & 0 \\
 & & & & & & & 2/15\,l_\mathrm{el}^2
\end{pmatrix}
\tag{1}
$$

describes the influence of axial load $F_x(t)$ on the beam-column's lateral stiffness. After the assembly of global mass and stiffness matrices from the element matrices, the inhomogeneous
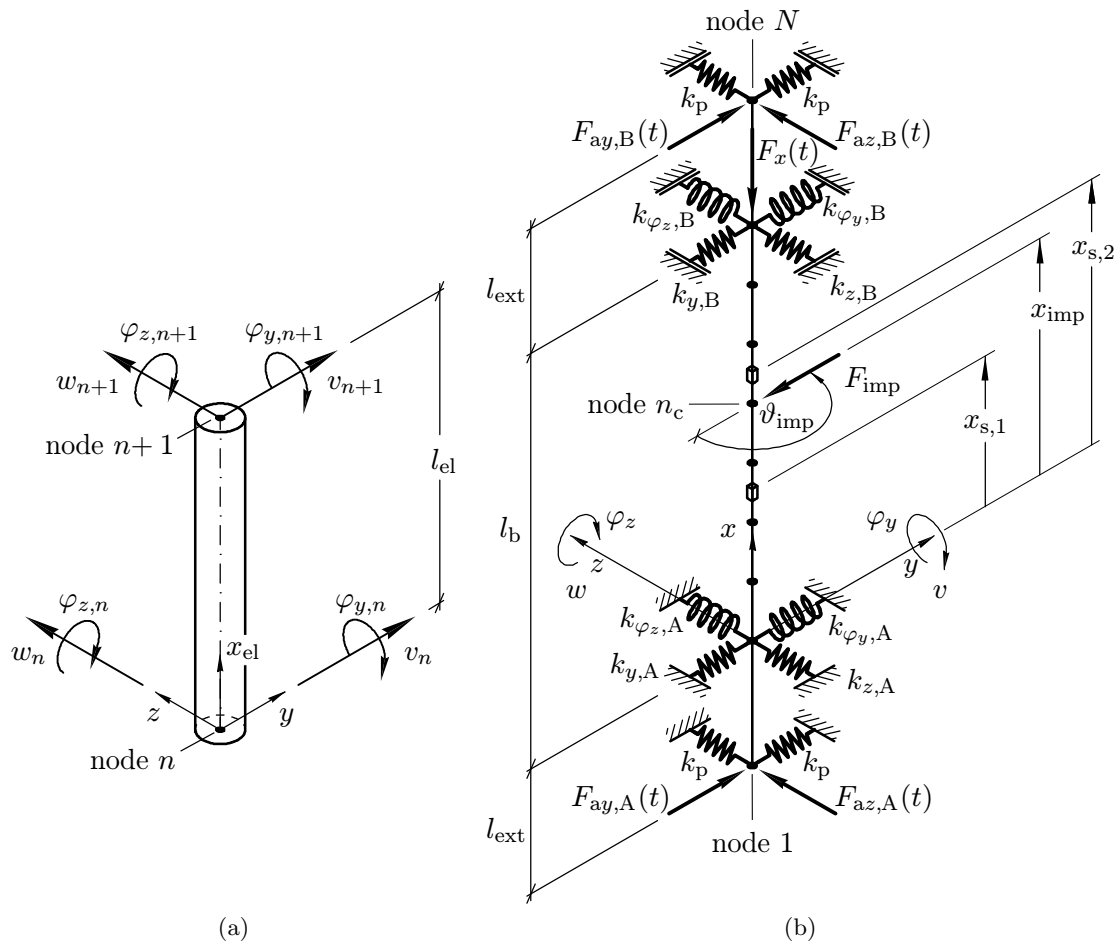
Figure 2: FE beam-column system, (a) n-th finite beam-column element of length l_{el} with element coordinates in positive directions, (b) FE model of beam-column.

FE equation of motion is

$$\boldsymbol{M}\,\ddot{\boldsymbol{r}}(t) + \boldsymbol{D}\,\dot{\boldsymbol{r}}(t) + \left(\boldsymbol{K}_{e} - F_x(t)\,\boldsymbol{K}_{g}\right)\boldsymbol{r}(t) = \boldsymbol{B}_0\,\boldsymbol{u}(t) + \boldsymbol{b}_{\mathrm{imp},0}\,F_{\mathrm{imp}} \tag{2}$$

with the $[4N \times 1]$ FE displacement vector

$$\boldsymbol{r}(t) = [v_1(t), w_1(t), \varphi_{y,1}(t), \varphi_{z}(t), \ldots, v_N(t), w_N(t), \varphi_{y,N}(t), \varphi_{z,N}(t)]^T . \tag{3}$$

The left side of (2) represents the ideal or perfect axially loaded beam-column with piezo-elastic supports. $\boldsymbol{M}$ is the global mass matrix, $\boldsymbol{D}$ is the global damping matrix, $\boldsymbol{K}_{e}$ is the global elastic stiffness matrix and $\boldsymbol{K}_{g}$ is the global geometric stiffness matrix, all $[4N \times 4N]$. The right side of (2) represents the external forces acting on the beam-column. These are caused, on the one hand, by the active control forces that are summarized in control input vector

$$\boldsymbol{u}(t) = \begin{bmatrix} F_{\mathrm{a}y,\mathrm{A}}(t) \\ F_{\mathrm{a}z,\mathrm{A}}(t) \\ F_{\mathrm{a}y,\mathrm{B}}(t) \\ F_{\mathrm{a}z,\mathrm{B}}(t) \end{bmatrix} \tag{4}$$

and, on the other hand, by the constant imperfection force F_{imp} with angle ϑ_{imp} that is used to include the effect of imperfections without changing the FE matrices on the left side of (2). The external forces are allocated to the FE nodes by the $[4N \times 4]$ control input matrix and the $[4N \times 1]$ imperfection input vector

$$
\boldsymbol{B}_0 = \underbrace{\begin{bmatrix} 1 & 0 & 0 & 0 \\ 0 & 1 & 0 & 0 \\ \vdots & \vdots & \vdots & \vdots \\ 0 & 0 & 1 & 0 \\ 0 & 0 & 0 & 1 \\ 0 & 0 & 0 & 0 \\ 0 & 0 & 0 & 0 \end{bmatrix}}_{[4N \times 4]} \quad \text{and} \quad \boldsymbol{b}_{\text{imp},0} = \underbrace{\begin{bmatrix} 0 \\ \vdots \\ 0 \\ \cos \vartheta_{\text{imp}} \\ \sin \vartheta_{\text{imp}} \\ 0 \\ \vdots \\ 0 \end{bmatrix}}_{[4N \times 1]} \tag{5}
$$

This way, the control input vector acts on the first and last nodes $n = 1$ and $n = N$ and the imperfection force acts on the central node $n = n_c$ of the FE model.

The stiffness matrix $\boldsymbol{K}_{\text{e}}$ in (2) includes the discrete stiffness k_{p}, k_{l} and k_{r} of piezoelectric stack actuators and elastic spring elements, table 1. The lateral stiffness k_{p} is added to the entries of the lateral degrees of freedom of nodes $n = 1$ and $n = N$. Similarly, the lateral and rotational stiffness k_{l} and k_{r} are added to the entries of the lateral and rotational degrees of freedom of nodes $n = 2$ and $n = N - 1$, figure 2b. The damping matrix $\boldsymbol{D}$ is assumed by RAYLEIGH proportional damping $\boldsymbol{D} = \alpha\,\boldsymbol{M} + \beta\,\boldsymbol{K}_{\text{e}}$, [14]. The proportional damping coefficients α and β are determined for experimentally identified modal damping ratios $\zeta_{1/2}$ of the first two bending modes.

The beam-column's lateral displacements $v(t)$ and $w(t)$ in a real test setup scenario are not measured directly. Four strain gauges at each of the two strain gauge positions $x_{\text{s},1/2}$ measure the surface strains due to bending in y- and z-direction, figure 1. Therefore, in the mathematical model, the surface strains in y- and z-direction at the strain gauge positions are chosen as output

$$
\boldsymbol{y}(t) = \begin{bmatrix} \varepsilon_y(x_{\text{s},1}, t) \\ \varepsilon_z(x_{\text{s},1}, t) \\ \varepsilon_y(x_{\text{s},2}, t) \\ \varepsilon_z(x_{\text{s},2}, t) \end{bmatrix} = \boldsymbol{C}_0\,\boldsymbol{r}(t). \tag{6}
$$

In (6), the $[4 \times 4N]$ output matrix $\boldsymbol{C}_0$ allocates the surface strains $\boldsymbol{y}(t)$ to the FE displacement vector (3) by the entries $-r_{\text{b}}\,\boldsymbol{g}''(x_{\text{s},1/2})$ at the FE nodes surrounding strain gauge positions $x_{\text{s},1/2}$. r_{b} is the beam-column radius and $\boldsymbol{g}''(x_{\text{s},1/2})$ is the second derivative of the HERMITIAN shape functions at the strain gauge positions, [12].

For convenience, (2) and (6) are written in state space representation

$$
\dot{\boldsymbol{x}}_{\text{FE}}(t) = \underbrace{\left(\begin{bmatrix} \boldsymbol{0} & \boldsymbol{I} \\ -\boldsymbol{M}^{-1}\,\boldsymbol{K}_{\text{e}} & -\boldsymbol{M}^{-1}\,\boldsymbol{D} \end{bmatrix} + F_x(t) \begin{bmatrix} \boldsymbol{0} & \boldsymbol{0} \\ \boldsymbol{M}^{-1}\,\boldsymbol{K}_{\text{g}} & \boldsymbol{0} \end{bmatrix} \right)}_{[8N \times 8N]} \boldsymbol{x}_{\text{FE}}(t)
$$

$$
+ \underbrace{\begin{bmatrix} \boldsymbol{0} \\ \boldsymbol{M}^{-1}\,\boldsymbol{B}_0 \end{bmatrix}}_{[8N \times 4]} \boldsymbol{u}(t) + \underbrace{\begin{bmatrix} \boldsymbol{0} \\ \boldsymbol{M}^{-1}\,\boldsymbol{b}_{\text{imp},0} \end{bmatrix}}_{[8N \times 1]} F_{\text{imp}} \tag{7}
$$

$$
\boldsymbol{y}(t) \;\; = \underbrace{\begin{bmatrix} \boldsymbol{C}_0 & \boldsymbol{0} \end{bmatrix}}_{[4 \times 8N]} \boldsymbol{x}_{\text{FE}}(t),
$$

with $[8N \times 1]$ FE state vector $\boldsymbol{x}_{\text{FE}}(t) = [\boldsymbol{r}(t), \dot{\boldsymbol{r}}(t)]^T$ and zero and identity matrices $\boldsymbol{0}$ and $\mathbf{I}$ of appropriate dimensions. In short form, (7) can be written as

$$\begin{aligned}
\dot{\boldsymbol{x}}_{\text{FE}}(t) &= \boldsymbol{A}_{\text{FE}}(F_x(t))\, \boldsymbol{x}_{\text{FE}}(t) + \boldsymbol{B}_{\text{FE}}\, \boldsymbol{u}(t) + \boldsymbol{b}_{\text{imp}}\, F_{\text{imp}} \\
\boldsymbol{y}(t) &= \boldsymbol{C}_{\text{FE}}\, \boldsymbol{x}_{\text{FE}}(t)
\end{aligned} \tag{8}$$

representing the full FE state space model of the beam-column with piezo-elastic supports, including imperfections, active control forces and sensor output. The influence of a time-varying axial load $F_x(t)$ on the dynamic system behavior is described by the system matrix $\boldsymbol{A}_{\text{FE}}(F_x(t))$.

3. Controller design
In the following, first a reduced modal model of the axially loaded beam-column is presented. Second, the modal model is augmented to include integrated states and a LQR for active buckling control is derived. As simplifications and in accordance with the controller of a real test setup, the imperfection force F_{imp} is ignored and the ideal beam-column system is used for controller design. Furthermore, the axial load $F_x(t)$ is assumed to be constant.

3.1. Reduced modal model
For the full state FE model (2) and as a specific example according to figure 2b, a number of $N = 35$ nodes resulting in $4N = 140$ degrees of freedom is chosen to properly describe the maximum surface strains at the strain gauge positions $x_{\text{s},1/2}$, (6). For controller design, however, the FE model is reduced by modal truncation to include the first two modes $q_1(t)$ and $q_2(t)$ for both y- and z-direction only. Consequently, the FE displacement vector (3) and the deformation of the imperfect beam-column is approximated by modal displacements

$$\boldsymbol{q}_{\text{m}}(t) = \begin{bmatrix} q_{1,y}(t) \\ q_{1,z}(t) \\ q_{2,y}(t) \\ q_{2,z}(t) \end{bmatrix} \tag{9}$$

via the transformation

$$\boldsymbol{r}(t) \approx \boldsymbol{\Phi}\, \boldsymbol{q}_{\text{m}}(t). \tag{10}$$

The $[4N \times 4]$ modal matrix

$$\boldsymbol{\Phi} = [\widehat{\boldsymbol{r}}_{1,y}, \widehat{\boldsymbol{r}}_{1,z}, \widehat{\boldsymbol{r}}_{2,y}, \widehat{\boldsymbol{r}}_{2,z}] \tag{11}$$

includes the first two $[4N \times 1]$ eigenvectors $\widehat{\boldsymbol{r}}_1$ and $\widehat{\boldsymbol{r}}_2$ in y- and z-direction of the FE model, [15]. The eigenvectors in (11) are normalized with respect to mass matrix $\boldsymbol{M}$ leading to the modal mass matrix $\widetilde{\boldsymbol{M}}$, modal elastic stiffness matrix $\widetilde{\boldsymbol{K}}_{\text{e}}$, modal geometric stiffness matrix $\widetilde{\boldsymbol{K}}_{\text{g}}$ and modal damping matrix $\widetilde{\boldsymbol{D}}$

$$\begin{aligned}
\widetilde{\boldsymbol{M}} &= \boldsymbol{\Phi}^T\, \boldsymbol{M}\, \boldsymbol{\Phi} = \mathbf{I} \\
\widetilde{\boldsymbol{K}}_{\text{e}} &= \boldsymbol{\Phi}^T\, \boldsymbol{K}_{\text{e}}\, \boldsymbol{\Phi} \\
\widetilde{\boldsymbol{K}}_{\text{g}} &= \boldsymbol{\Phi}^T\, \boldsymbol{K}_{\text{g}}\, \boldsymbol{\Phi} \\
\widetilde{\boldsymbol{D}} &= \boldsymbol{\Phi}^T\, \boldsymbol{D}\, \boldsymbol{\Phi}
\end{aligned} \tag{12}$$

with the identity matrix $\mathbf{I}$, all $[4 \times 4]$. Using the $[8 \times 1]$ modal state vector with the modal displacements and velocities

$$\boldsymbol{x}_{\text{m}}(t) = \begin{bmatrix} \boldsymbol{q}_{\text{m}}(t) \\ \dot{\boldsymbol{q}}_{\text{m}}(t) \end{bmatrix}, \tag{13}$$

the first order modal state space equations for the ideal axially loaded beam-column with constant axial load $F_x(t) = F_x = \mathrm{const}$ are

$$
\dot{\boldsymbol{x}}_{\mathrm{m}}(t) = \underbrace{\left(\begin{bmatrix} \mathbf{0} & \mathbf{I} \\ -\widetilde{\boldsymbol{K}}_{\mathrm{e}} & -\widetilde{\boldsymbol{D}} \end{bmatrix} + F_x \begin{bmatrix} \mathbf{0} & \mathbf{0} \\ \widetilde{\boldsymbol{K}}_{\mathrm{g}} & \mathbf{0} \end{bmatrix} \right)}_{[8\times 8]} \boldsymbol{x}_{\mathrm{m}}(t) + \underbrace{\begin{bmatrix} \mathbf{0} \\ \boldsymbol{\Phi}^T \boldsymbol{B}_0 \end{bmatrix}}_{[8\times 4]} \boldsymbol{u}(t)
$$

$$
\boldsymbol{y}(t) = \underbrace{\begin{bmatrix} \boldsymbol{C}_0 \boldsymbol{\Phi} & \mathbf{0} \end{bmatrix}}_{[4\times 8]} \boldsymbol{x}_{\mathrm{m}}(t),
\tag{14}
$$

[15]. (14) can also be written in short form

$$
\begin{aligned}
\dot{\boldsymbol{x}}_{\mathrm{m}}(t) &= \boldsymbol{A}_{\mathrm{m}}(F_x)\, \boldsymbol{x}_{\mathrm{m}}(t) + \boldsymbol{B}_{\mathrm{m}}\, \boldsymbol{u}(t) \\
\boldsymbol{y}(t) &= \boldsymbol{C}_{\mathrm{m}}\, \boldsymbol{x}_{\mathrm{m}}(t).
\end{aligned}
\tag{15}
$$

3.2. Integral LQR

Active buckling control of the circular beam-column is achieved by an infinite horizon, continuous-time linear quadratic regulator (LQR). The constant imperfection force F_{imp} that represents imperfections such as predeformation, eccentric loading or clamping moments in the FE model (8) is not explicitly included in the controller modal model (15). In a standard LQR design as performed in [10], the imperfection force leads to a constant controller error and non-zero beam-column deformation despite of the active buckling control. High static controller gains that might prove problematic for time-varying axial loads are necessary in order to reduce the beam-column deformation close to zero. To avoid this, an additional integral term is included in the controller design. For that, the modal state vector (13) is augmented by the integral of the modal displacements

$$
\boldsymbol{x}_{\mathrm{i}}(t) = \int \boldsymbol{q}_{\mathrm{m}}(t)\, \mathrm{d}t
\tag{16}
$$

to get the new $[12 \times 1]$ state vector

$$
\boldsymbol{x}(t) = \begin{bmatrix} \boldsymbol{x}_{\mathrm{m}}(t) \\ \boldsymbol{x}_{\mathrm{i}}(t) \end{bmatrix},
\tag{17}
$$

[16, 17]. With the first derivative of the new state vector

$$
\dot{\boldsymbol{x}}_{\mathrm{i}}(t) = \boldsymbol{q}_{\mathrm{m}}(t) = \underbrace{\begin{bmatrix} \mathbf{I} & \mathbf{0} \end{bmatrix}}_{[4\times 8]} \boldsymbol{x}_{\mathrm{m}}(t),
\tag{18}
$$

the augmented state space system including the integral term can be written as

$$
\dot{\boldsymbol{x}}(t) = \underbrace{\begin{bmatrix} \boldsymbol{A}_{\mathrm{m}}(F_x) & \mathbf{0} \\ \begin{bmatrix} \mathbf{I} & \mathbf{0} \end{bmatrix} & \mathbf{0} \end{bmatrix}}_{[12\times 12]} \boldsymbol{x}(t) + \underbrace{\begin{bmatrix} \boldsymbol{B}_{\mathrm{m}} \\ \mathbf{0} \end{bmatrix}}_{[12\times 4]} \boldsymbol{u}(t)
$$

$$
\boldsymbol{y}(t) = \underbrace{\begin{bmatrix} \boldsymbol{C}_{\mathrm{m}} & \mathbf{0} \end{bmatrix}}_{[4\times 12]} \boldsymbol{x}(t).
\tag{19}
$$

In short form, the final state space system (19) of the ideal axially loaded beam-column with piezo-elastic supports for controller design is

$$
\begin{aligned}
\dot{\boldsymbol{x}}(t) &= \boldsymbol{A}(F_x)\, \boldsymbol{x}(t) + \boldsymbol{B}\, \boldsymbol{u}(t) \\
\boldsymbol{y}(t) &= \boldsymbol{C}\, \boldsymbol{x}(t),
\end{aligned}
\tag{20}
$$

with system matrix $\boldsymbol{A}(F_x)$, input matrix $\boldsymbol{B}$ and output matrix $\boldsymbol{C}$. The control law of the LQR determines the control input $\boldsymbol{u}(t)$ so that the quadratic performance index

$$J = \int_0^\infty \left\{ \boldsymbol{x}^T(t)\,\boldsymbol{Q}\,\boldsymbol{x}(t) + \boldsymbol{u}^T(t)\,\boldsymbol{R}\,\boldsymbol{u}(t) \right\} \mathrm{d}t \tag{21}$$

is minimized, [17]. The $[12 \times 12]$ matrix $\boldsymbol{Q}$ includes weights on system state vector $\boldsymbol{x}(t)$ and is chosen as diagonal matrix with largest weights on the modal displacements of the first modes in y- and z-direction and their integrals, [18]. The $[4 \times 4]$ matrix $\boldsymbol{R}$ includes weights on control input $\boldsymbol{u}(t)$ and is chosen as identity matrix. The control input (4) is calculated by

$$\boldsymbol{u}(t) = -\boldsymbol{K}_{\mathrm{LQR}}(F_x)\,\boldsymbol{x}(t), \tag{22}$$

where the $[4 \times 12]$ control matrix $\boldsymbol{K}_{\mathrm{LQR}}(F_x)$ is given by

$$\boldsymbol{K}_{\mathrm{LQR}}(F_x) = \boldsymbol{R}^{-1}\,\boldsymbol{B}^T\,\boldsymbol{P}(F_x). \tag{23}$$

In (23), $\boldsymbol{P}(F_x)$ is the solution of the continuous-time Algebraic RICCATI Equation (CARE)

$$\boldsymbol{A}(F_x)^T\,\boldsymbol{P}(F_x) + \boldsymbol{P}(F_x)\,\boldsymbol{A}(F_x) - \boldsymbol{P}(F_x)\,\boldsymbol{B}\,\boldsymbol{R}^{-1}\,\boldsymbol{B}^T\,\boldsymbol{P}(F_x) + \boldsymbol{Q} = 0 \tag{24}$$

with system matrix $\boldsymbol{A}(F_x)$, input matrix $\boldsymbol{B}$, (20), and weights $\boldsymbol{Q}$ and $\boldsymbol{R}$, [17]. Since the system matrix is a function of axial load F_x, the solution of (24) and the optimal control matrix (23) also depend on the axial load. In the numerical simulations, therefore, the control matrix is switched between different control matrices which are calculated for constant axial loads $F_x = 0 - 3\,500\,\mathrm{N}$ in steps of $500\,\mathrm{N}$.

4. Numerical simulation of active buckling control
In this section, numerical simulations of the active buckling control are presented to show the stabilization capability of the investigated system. First, the theoretical buckling behavior of the ideal beam-column system is presented. Second, active buckling control of the imperfect beam-column system is investigated.

4.1. Buckling behavior of ideal beam-column system
The left side of (2) determines the dynamic behavior of the ideal, perfect beam-column. Without imperfections or other external disturbances, the beam-column will not deform and remains in straight position regardless of the applied axial load $F_x(t)$. For certain axial loads, the theoretical buckling loads, the matrix $\boldsymbol{K}_{\mathrm{e}} - F_x(t)\,\boldsymbol{K}_{\mathrm{g}}$ becomes singular and the system is instable. Consequently, the theoretical buckling loads for the homogeneous beam-column model in (2) with piezo-elastic supports are the eigenvalues of the eigenvalue problem

$$\det\left[\boldsymbol{K}_{\mathrm{e}} - F_x\,\boldsymbol{K}_{\mathrm{g}}\right] = 0, \tag{25}$$

[13]. The lowest eigenvalue calculated for the given boundary conditions, table 1, is the critical buckling load $F_{x,cr} = 3\,206\,\mathrm{N}$. The beam-column with circular cross-section has no preferred direction of buckling, so the beam-column may buckle in any plane lateral to the x-axis.

4.2. Buckling behavior of imperfect beam-column system

In a real, imperfect beam-column, the applied axial compressive load $F_x(t)$ increases the initial deformation. In the numerical simulations, the dynamic behavior of the real beam-column resembles the dynamic behavior of the FE model (8) with the constant imperfection force F_{imp} acting at node $n_{\text{c}} = 18$, figure 2b, that is used to initially deform the beam-column. For that, figure 3 shows a block diagram for the numerical simulations. The axial load $F_x(t)$ acts on node $n = 34$ of the beam-column as a slow ramp to represent a quasi-static loading as in a real test setup.
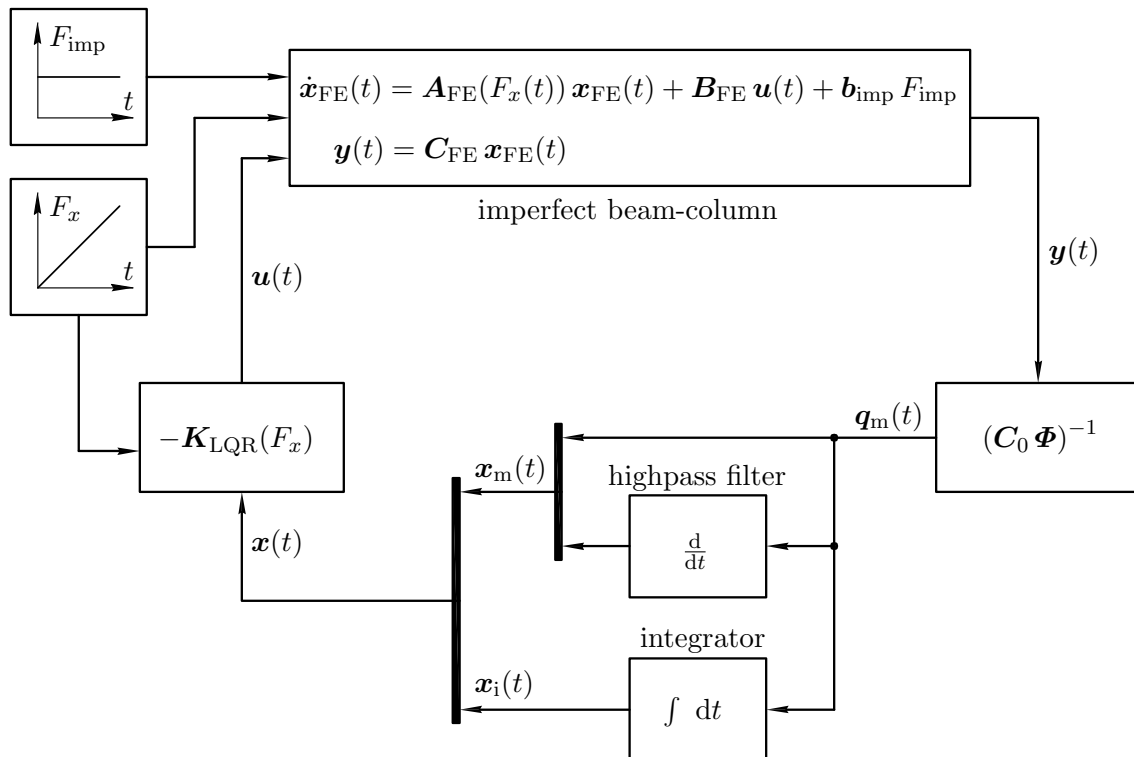

Figure 3: Block diagram for numerical simulation of active buckling control.

In figure 3, the surface strains $\varepsilon_{y/z}$ according to (6) are the output $\boldsymbol{y}(t)$ of the FE model (8). The deformation of the beam-column in y- and z- direction due to the axial load $F_x(t)$ and the external forces F_{imp} and $\boldsymbol{u}(t)$ is approximated by the modal displacements (9) that, due to the invertibility of the $[4 \times 4]$ matrix $(\boldsymbol{C}_0\,\boldsymbol{\Phi})$, result in

$$\boldsymbol{q}_{\text{m}}(t) = (\boldsymbol{C}_0\,\boldsymbol{\Phi})^{-1}\,\boldsymbol{y}(t). \tag{26}$$

A first order BUTTERWORTH highpass filter is used to numerically differentiate the modal displacements $\boldsymbol{q}_{\text{m}}(t)$ to get the modal velocities $\dot{\boldsymbol{q}}_{\text{m}}(t)$ that together form the modal state vector $\boldsymbol{x}_{\text{m}}(t)$, (13). An integrator sums up the modal displacements to get the integral state vector $\boldsymbol{x}_{\text{i}}(t)$, (16). The full state vector $\boldsymbol{x}(t)$, (17) is used to calculate the control forces $\boldsymbol{u}(t)$ via (22). The control matrix $\boldsymbol{K}_{\text{LQR}}(F_x)$, (23) is calculated for the reduced ideal modal model (20) and for constant axial loads F_x. For the quasi-statically increasing axial load $F_x(t)$, the control matrix is switched in steps of $5\,\text{N}$.

The results of the numerical simulations with and without active buckling control for a constant imperfection force $F_{\text{imp}} = 2\,\text{N}$ with angle $\vartheta_{\text{imp}} = 234°$ and an axial load ramp

$F_x(t) = 0 - 3\,400\,\text{N}$ are shown in figure 4. Again, the number of nodes for this example and according to figure 2b is $N = 35$. This leads to the absolute displacement of the central node $n_\text{c} = 18$ with nodal displacements $v_{18}(t)$ and $w_{18}(t)$ in y- and z-direction that is plotted with respect to the axial load $F_x(t)$ in figure 4a. Figure 4b shows the displacements $v_{18}(t)$ and $w_{18}(t)$ of the central FE node in the y-z-plane.
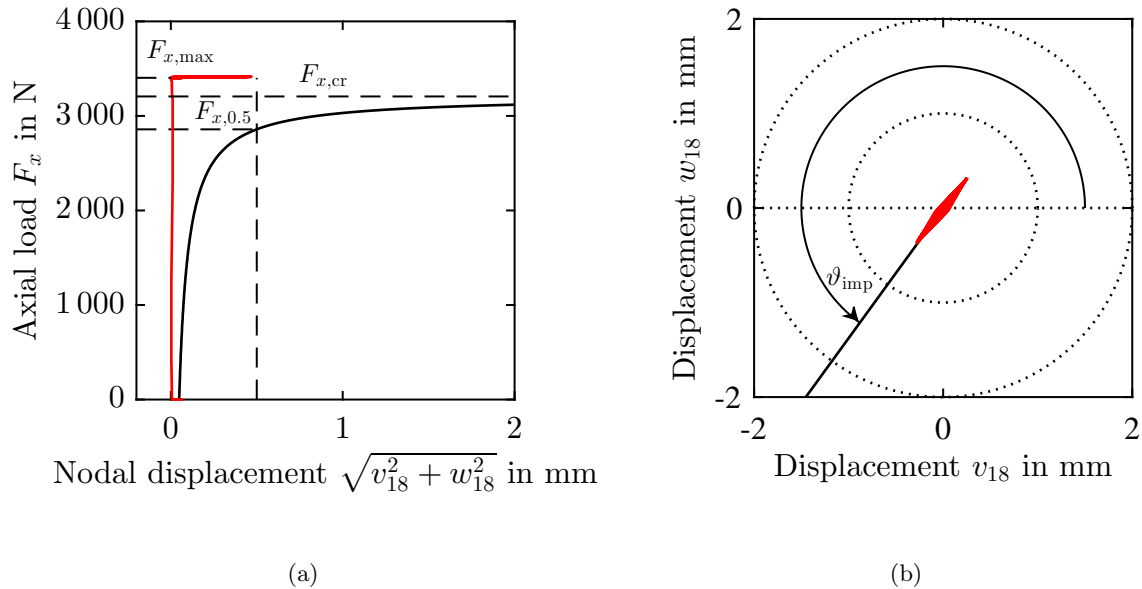

(a)   (b)

Figure 4: Displacements $v_{18}(t)$ and $w_{18}(t)$ of the central node $n_\text{c} = 18$ in y- and z-direction for the imperfect beam-column with (——) and without (——) active buckling control, (a) absolute displacement versus axial load $F_x(t)$ (b) displacements in y-z-plane.

Without active buckling control, the load deformation curve shows the typical continuous deformation with increasing axial load. That is known from real, imperfect beam-columns where sudden buckling does not occur, [1]. The beam-column continuously deforms in the direction of the constant lateral disturbance ϑ_imp. It is not possible to define one single critical buckling load of the uncontrolled system, only a maximum bearable load is seen for a given admissible deformation. A maximum absolute displacement of $0.5\,\text{mm}$ is reached for the axial load of $F_{x,0.5} = 2\,858\,\text{N} = 0.89\,F_{x,cr}$, figure 4a. That is considerably less than the theoretical critical buckling load $F_{x,cr} = 3\,206\,\text{N}$, determined for the ideal beam-column system.

With active buckling control, the active forces at nodes $n = 1$ and $n = 35$, with respect to figure 2b, are able to initially force the beam-column into a straight position and then to reduce the beam-column deformation for the quasi-statically increasing axial load $F_x(t)$. The integral LQR is able to stabilize the beam-column up to an axial load of $F_{x,\max} = 3\,360\,\text{N} \approx 1.05\,F_{x,cr}$. Up to $F_{x,\max}$, the deformation in both y- and z-direction remains zero, figure 4a. At $F_{x,cr}$, the system matrix $\boldsymbol{A}_\text{FE}(F_x(t))$ of the FE beam-column model (8) becomes instable and the controller is able to stabilize the beam-column and keep it in its straight position. At $F_{x,\max}$ however, oscillation of higher modes that are not considered in the controller occur that grow and finally lead to buckling of the beam-column at an angle of ϑ_imp so that the simulation is stopped at $F_x(t) = 3\,400\,\text{N}$. Nevertheless, the presented active buckling control is able to stabilize the beam-column and to increase the maximum bearable load above the theoretical critical buckling load $F_{x,cr}$.

5. Conclusions

A new method of active buckling control of an imperfect axially loaded beam-column with circular cross-section by piezo-elastic supports is presented and investigated numerically. Imperfections are represented by a constant lateral imperfection force that initially deforms the beam-column. With the piezo-elastic supports, lateral forces of piezoelectric stack actuators are transformed into bending moments acting in arbitrary directions at the beam-column ends. A finite element (FE) model of the imperfect beam-column system is derived and used for numerical simulations. A reduced modal model of the ideal beam-column is augmented by integrated states and used to implement an integral linear quadratic regulator (LQR). Without active buckling control, the numerical simulations show that the imperfect axially loaded beam-column exhibits high lateral deformations for axial loads considerably below the theoretical critical buckling load of the ideal structure. With active buckling control using piezo-elastic supports, stabilization above the theoretical critical buckling load and the maximum bearable load of the passive imperfect beam-column is possible. In current investigations, the practical effectiveness of the stabilization concept is tested in an experimental setup.

Acknowledgments

References
[1] Timoshenko S P and Gere J M 1961 *Theory of Elastic Stability* (McGraw-Hill, New York)
[2] Meressi T and Paden B 1993 *Journal of Guidance, Control, and Dynamics* **16** 977–980
[3] Wang Q S 2010 *Smart Materials and Structures* **19** 1–8
[4] Thompson S P and Loughlan J 1995 *Composite Structures* **32** 59–67
[5] Berlin A A, Chase J G, Yim M, Maclean J B, Olivier M and Jacobsen S C 1998 *Journal of Intelligent Material Systems and Structures* **9** 574–586
[6] Zenz G and Humer A 2015 *Acta Mechanica* **226** 3961–3976
[7] Enss G C, Platz R and Hanselka H 2012 *Shock and Vibration* **19** 929–937
[8] Enss G C and Platz R 2014 *Topics in Modal Analysis I, Volume 7: Proceedings of the 32nd IMAC, A Conference and Exposition on Structural Dynamics, 2014* 209 ed Clerck J D (Springer International Publishing) pp 291–297
[9] Schaeffner M, Enss G C and Platz R 2014 *Proceedings of SPIE Vol. 9057 Active and Passive Smart Structures and Integrated Systems* (San Diego, CA/USA) p 90572H sPIE Smart Structures/NDE 2014
[10] Schaeffner M, Platz R and Melz T 2015 *Proceedings of SMART2015 7th ECCOMAS Thematic Conference on Smart Structures and Materials* (Ponta Delgada, Azores)
[11] Götz B, Schaeffner M, Platz R and Melz T 2015 *Applied Mechanics and Materials, Trans Tech Publications* **807** 67–77
[12] Klein B 2012 *FEM* (Springer Vieweg, Wiesbaden)
[13] Przemieniecki J S 1968 *Theory of Matrix Structural Analysis* (McGraw-Hill, New York)
[14] Khot S M and Yelve N P 2010 *Journal of Vibration and Control* **0** 1–6
[15] Gawronski W 2010 *Advanced Structural Dynamic and Active Control of Structures* (Springer)
[16] Hendricks E, Jannerup O and Sørensen P H 2008 *Linear Systems Control* (Springer)
[17] Skogestad S and Postlethwaite I 2005 *Multivariable Feedback Control: Analysis and Design* (John Wiley & Sons, New York)
[18] Lunze J 2008 *Regelungstechnik 2 Mehrgrößensysteme, Digitale Regelung* (Springer-Verlag Berlin Heidelberg)